Normal modes and long period seismograms in a 3D anelastic elliptical rotating Earth

Raphaële Millot-Langet, Eric Clévédé, Philippe Lognonné

Normal modes and long period seismograms in a 3D anelastic elliptical rotating Earth

Raphaële Millot-Langet,[1,2] Eric Clévédé,[2] and Philippe Lognonné[1]

Received 9 September 2002; revised 19 December 2002; accepted 30 January 2003; published 5 March 2003.

[1] We present results of a direct method to compute realistic long period (>200 s in this example) synthetic seismograms using higher order perturbation theory (up to the 3rd order). Normal modes are computed for the Earth, taking into account rotation, ellipticity, 3D elastic lateral heterogeneities (SAW12D) for the whole mantle, and anelastic lateral variations in the upper mantle (QR19). Coupling between different modes and branches is included in the computation. We study the sensitivity of the waveform to 3D anelasticity and the biases between 3D elastic and 3D anelastic variations. The resulting seismograms can be computed to higher frequency and may then be used to perform whole mantle joint inversions for elastic and anelastic structure. *INDEX TERMS:* 7207 Seismology: Core and mantle; 7255 Seismology: Surface waves and free oscillations; 7260 Seismology: Theory and modeling. **Citation:** Millot-Langet, R., E. Clévédé, and P. Lognonné, Normal modes and long period seismograms in a 3D anelastic elliptical rotating Earth, *Geophys. Res. Lett.*, *30*(5), 1202, doi:10.1029/2002GL016257, 2003.

1. Introduction

[2] Today's seismology has given us a refined knowledge on the Earth's elastic behavior. There are strong constraints on its spherical structure and 3D mantle models keep increasing in resolution thanks to the huge effort made in data processing and theory refinements. Still, while the localization and sign of the heterogeneities are rather stable, the amplitude of the anomalies is not very well constrained. Moreover, some data, full of information, are still rejected because they are too anomalous to be included in regular inversion datasets [*Lay and Kanamori*, 1985; *Woodhouse and Wong*, 1986].

[3] The anelastic features of the Earth remain poorly resolved. Although the spherical structure of attenuation is rather well known, its lateral variability is still challenging for seismologists. Only upper mantle models are available, for example in *Romanowicz* [1995] or *Selby and Woodhouse* [2002], and the amplitude of their anomalies is thought to be underestimated (Romanowicz, personal communication).

[4] The method we present in this paper allows the precise computation of the whole waveform, taking into account the competitive effects of elastic and anelastic structures, as well as the sometimes masking effect of rotation and ellipticity.

[5] We have decided to focus on low frequency modes because they have sensitivity down to the bottom of the mantle and are therefore good candidates to reveal the internal structure of the deep Earth. In this paper, we show results of the forward problem. We have computed normal modes (up to 5 mHz) for a 3D anelastic elliptical rotating Earth and corresponding seismograms.

2. Method

[6] The propagation equation is solved in the frequency domain using higher order perturbation theory. Complex eigenfrequencies and the corresponding eigenfunctions are found in the spherical case using 1D models, such as PREM [*Dziewonski and Anderson*, 1981] or 1066A [*Gilbert and Dziewonski*, 1975]. Perturbations are then added to the operator, and we compute the perturbed modes corresponding to the new model [*Lognonné*, 1991; *Lognonné and Clévédé*, 2002]. In this experiment, we have included the effect of lateral variations of elastic parameters, as well as lateral variations of the Q factor. We have also added rotation and ellipticity of figure in the computation, in the exact formulation described by *Dahlen and Tromp* [1998]. Perturbations are developed up to the 3rd order in frequency (and thus, second order in amplitude), in the non-dispersive approximation.

[7] We compute interaction matrices following the theory developped by *Woodhouse and Dahlen* [1978] and use Legendre transform [*Lognonné and Romanowicz*, 1990] to compute kernels for the 3D structure. For each coupling matrix, we compute its Frobenius norm ε which characterizes the coupling strength between modes: $\varepsilon_{kk'} = \| \frac{\langle k|\delta H|k'\rangle}{\omega_k^2 - \omega_{k'}^2} \|$, where δH is the perturbation to the Hamiltonian operator, and $\omega_{k,k'}$ the frequencies of the two coupled modes $|k>$ and $|k'>$. We keep only those with a big enough contribution.

[8] Contrary to other methods using asymptotic or high frequency approximations, the seismograms we compute have a real Fresnel zone (off-path sensitivity). They inherently take into account the focussing and defocussing effects due to elastic gradients. We compute receiver modulation functions for each station and source modulation functions for each earthquake and then combine them to give the seismograms [*Clévédé and Lognonné*, 1996]. As a result, the computation time increases as $N + M$ and not $N * M$ for N receivers and M sources.

3. Normal Modes

[9] We use PREM as the reference 1D model. We then add the effects of rotation, ellipticity, 3D elastic and 3D anelastic structures, introducing them at the same time or separately in order to assess the non linearity of the perturbation process. We have computed normal modes of

[1]Département de Géophysique Spatiale et Planétaire, Institut de Physique du Globe de Paris, France.
[2]Département de Sismologie, Institut de Physique du Globede Paris, France.

0094-8276/03/2002GL016257

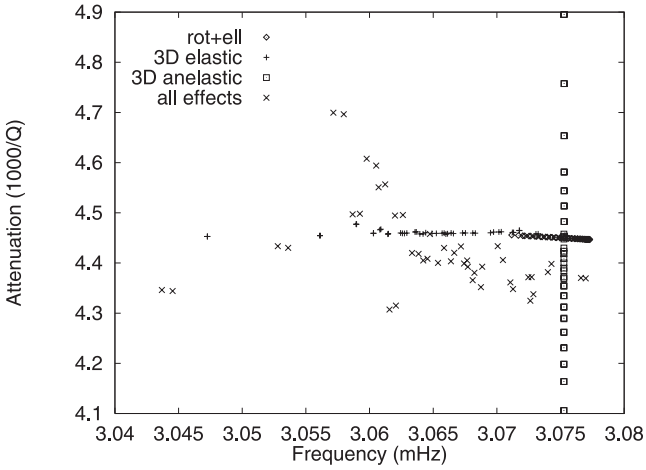

Figure 1. Splitting of the singlets of ${}_0S_{22}$. Rotation and ellipticity (diamonds) mainly act on frequency. The 3D elastic structure (crosses) controls the real part of frequency and the 3D anelastic structure (squares) controls the imaginary part, attenuation. The Xs show the result of these combined perturbations. Typical errors in the determination of the frequencies are of the order of 0.1‰, i.e. 0.3 μHz. The splitting width is about 35 μHz here.

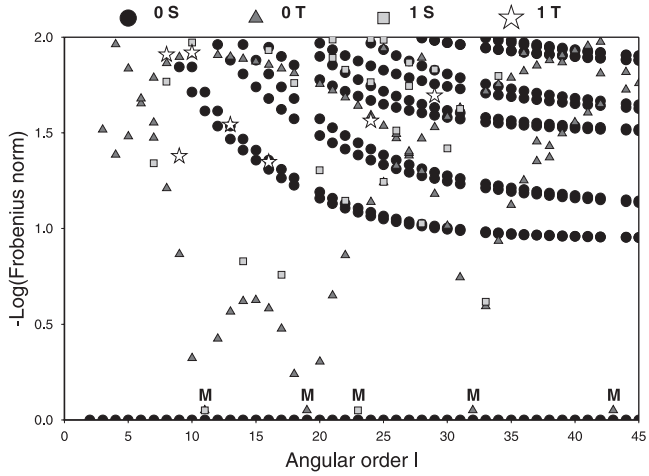

Figure 2. For each ℓ, we represent the Frobenius norm of the coupling matrix between mode ${}_0S_\ell$ and the modes from the four considered branches. For instance, black dots for a given ℓ correspond to the coupling strength of mode ${}_0S_\ell$ with the closest neighbours along the fundamental spheroidal branch. Modes indicated by an "M" are treated as supermultiplets.

the fundamental and first harmonic spheroidal and toroidal branches up to 5 mHz (200s). We have used SAW12D model [*Li and Romanowicz*, 1996] for the elastic lateral variations in the mantle, and QR19 model [*Romanowicz*, 1995] for the anelastic lateral variations in the upper mantle.

[10] Because of the selection rules, to first order, rotation and ellipticity couple modes with the same parity, up to $\Delta\ell = 2$. For example, mode ${}_nS_\ell$ is coupled with ${}_{n'}S_{\ell\pm2}$ and ${}_{n'}T_{\ell\pm1}$. The 3D elastic and anelastic structures (to 1st order) couple modes with an angular order difference $\Delta\ell$ no greater than the maximum degree of spherical harmonics present in the model. For example, since SAW12D is a degree 12 model, it is not necessary to couple modes with $\Delta\ell > 12$.

[11] We have first computed the fundamental spheroidal branch up to an angular order ℓ of 45 (5 mHz). Figure 1 shows the splitting pattern for mode ${}_0S_{22}$. As expected, rotation and ellipticity have the strongest effect for low frequencies (low angular order ℓ), the 3D elastic model creates splitting mostly on the real part of the frequency whereas the strongest effect of the 3D anelastic model in on the imaginary part.

[12] In order to optimize the computation time, we have looked at the strength of the coupling to reduce the number of modes to be taken into account. Figure 2 shows the coupling strength pattern for the fundamental spheroidal branch. For certain modes, especially at low frequencies, cross-branch coupling plays a prominent role. It is then critical to include it in the coupling scheme. *Resovsky and Ritzwoller* [1994] have worked in the same context, but could not include too many modes because of the heavy computational effort required in their Galerkin approach. They thus chose to include only along-branch coupling, up to $\Delta\ell = 5$, missing important coupling. Indeed, for 2/3 of these low frequency fundamental spheroidal modes, cross-coupling is stronger than along-branch coupling.

[13] Figure 3 shows the residual self-coupling splitting patterns for mode ${}_0S_{22}$, computed with different Frobenius cut-offs. If the coupling scheme is restricted to ±5 along the fundamental spheroidal branch, as in *Resovsky and Ritzwoller* [1994], the resulting splitting lacks the attenuation span due to cross-branch coupling, with toroidal modes in particular. In contrast, the perturbation method can easily include more modes in the computation and account for effects they did not study. We can then confirm their conclusions and try to go one step further, towards the inversion. We select the modes that are strongly coupled using the Frobenius norm as the criterion, within the range of modes allowed by the selection rules. We have limited

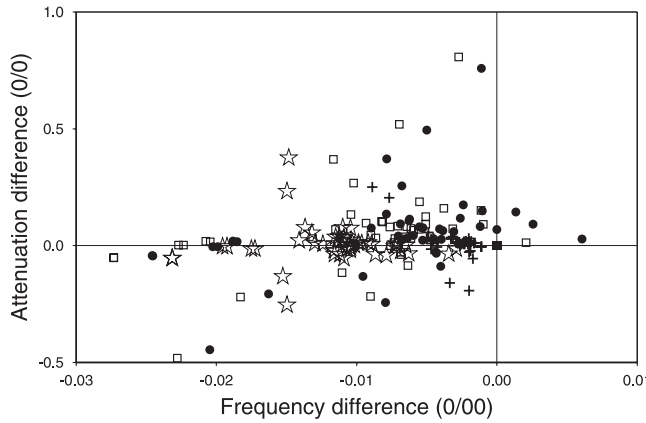

Figure 3. Residual splitting patterns for mode ${}_0S_{22}$. Self coupling (full squares) is the reference (thus all squares are superimposed on [0,0]). Crosses, circles and open squares correspond respectively to a 10^{-1} (2 modes), 10^{-2} (12 modes) and $10^{-2.4}$ (26 modes) Frobenius cut-off. The stars correspond to ±5 along-branch coupling (11 modes).

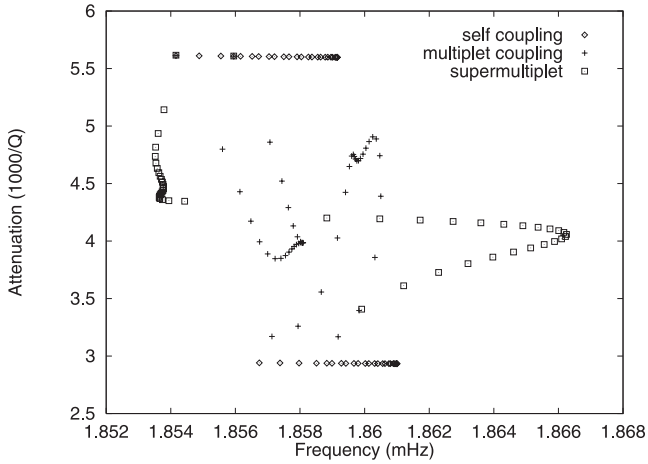

Figure 4. Splitting of the singlets of pair ${}_0S_{11}-{}_0T_{12}$ computed for only the effects of rotation and ellipticity, using the 1D reference model 1066A, to which attenuation is added. Classical perturbation theory (crosses) fails in this case of strong coupling but the supermultiplet case (squares) reproduces the results of Galerkin theory [*Masters et al.*, 1983].

ourselves in the further computations to coupling stronger than 10^{-2}, which is a rather satisfying compromise between accuracy and tractability.

[14] Although the discrepancies between those different splitting patterns may seem too small to ever be observed, it is important to notice that the real observation is made on the local frequency and amplitude, and the effect of coupling is enhanced when the excitation of the different singlets is taken into account. For instance, for the 3D elastic effect only, for mode ${}_0S_{22}$, the amplitude difference with respect to the 1D PREM reference is of 6% for self-splitting, 11% for a 10^{-1} Frobenius cut-off and 13% for a 10^{-2} Frobenius cut-off. As a comparison, the 3D anelastic structure yields a 19% difference between 1D PREM and self-splitting.

[15] The case of mode ${}_0S_{22}$ is representative of most of the modes but strong effects can be seen when two modes are very close in frequency. In such a resonant case, perturbation theory fails because the assumption that the effect should remain small is no longer valid. We then use a quasi-degenerate perturbation method, considering that all singlets of the two modes should be regarded as belonging to the same supermultiplet. Figure 4 shows the example of the splitting of ${}_0S_{11}-{}_0T_{12}$ pair in 1066A, due to rotation and ellipticity. With higher order perturbation theory using the supermultiplet case, we are able to reproduce the results obtained using full computation such as Galerkin theory or variational schemes [*Masters et al.*, 1983; *Park and Gilbert*, 1986]. Of course, this effect is very model-dependent since the frequencies of the modes are slightly shifted from one spherical model to an other. The supermultiplets considered in the example using PREM as the 1D model appear on Figure 2.

[16] Because spheroidal and toroidal modes are coupled through rotation, toroidal peaks can show up on vertical spectra [*Masters et al.*, 1983; *Zürn et al.*, 2000]. These observations can easily be accounted for using our calculation method of modes and seismograms. Figure 5 shows the example of the 1998/03/25 Balleny Islands earthquake (Mw = 7.8) recorded at GEOSCOPE station ECH.

[17] In order to compare the computational efficiency of the perturbation and the Galerkin methods, we have computed mode ${}_0S_{22}$, coupled with 7 other modes: ${}_0T_{23}$, ${}_0S_{23}$, ${}_0S_{21}$, ${}_2S_{14}$, ${}_0S_{24}$, ${}_0S_{20}$ and ${}_0T_{21}$, corresponding to a $10^{-1.7}$ Frobenius cut-off. The perturbation procedure was about 20 times faster than the Galerkin method. For both methods, the computation time increases as l^3, thus, for a given l_{max}, the computation of the last 15% of the considered branch takes as much time as the computation of the first 85%.

4. Seismograms and Spectra

[18] We compute spectra and corresponding seismograms using four different mode sets obtained using different Earth models. The first one is the 1-D anelastic PREM. The second one is the 3-D elastic SAW12D model superimposed on the PREM. The third one is the 3-D pure anelastic model QR19 superimposed on the PREM. The fourth one is the combination of SAW12D and QR19 models superimposed on the PREM.

[19] We chose the Harvard CMT solution for the 1995/07/30 Chile earthquake (Mw = 7.7) as source. Seismograms are computed for the vertical component of the GEOSCOPE station ATD with 70 hours duration, and low-pass filtered at 5 mHz.

[20] The resulting seismograms and spectra are shown on Figure 6. We chose to display the seismograms for a time window corresponding to the third Rayleigh train in order to clearly separate traces. Spectra are computed using the whole seismogram duration. This particular trace appears to be a extreme case with a 0.5% frequency shift for most of the modes, which is not among the most common observations. It samples one of the strongest low velocity anomalies of the model.

[21] In the spectral domain, the coupling effect is clear on the example of modes ${}_0S_{26}$, ${}_1S_{17}$ and ${}_0S_{27}$. These three

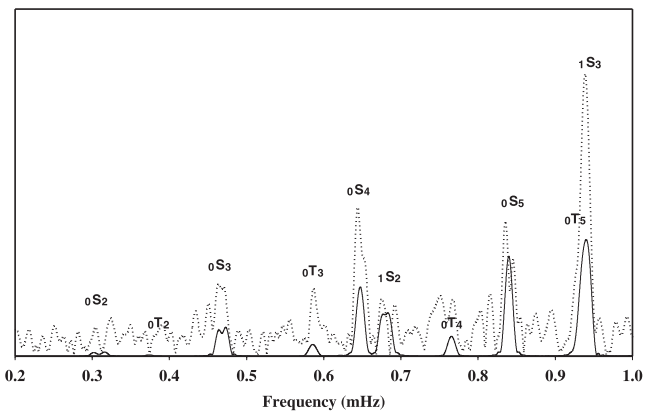

Figure 5. Spectrum of a 48 hour long vertical record at station ECH for the Balleny Islands 1998 earthquake. The synthetic (solid) computed with only the effect of rotation accounts for the toroidal peaks (${}_0T_3$ and ${}_0T_4$) that appear on the data (dotted). Also note the splitting of ${}_0S_3$ for example, seen both on the data and synthetic. In this frequency range, rotation is the most efficient coupling and splitting mechanism.

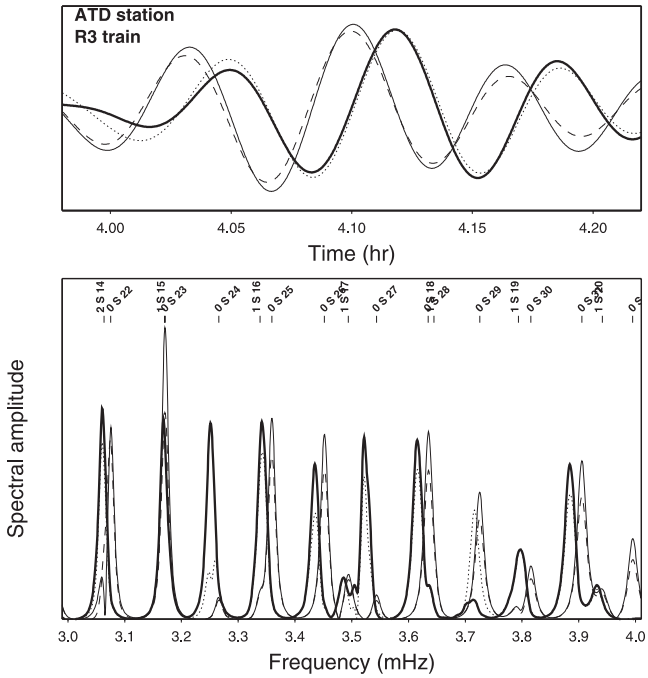

Figure 6. Top: R3 train from synthetic seismograms for the Antofagasta earthquake at station ATD, computed in four models: PREM (thin solid), SAW12D alone (thick solid), QR19 alone (dashed) and SAW12D + QR19 (dotted). Bottom: Corresponding amplitude spectra. The PREM frequencies are shown for the modes used in the computation. See text for details.

modes are clearly separated in the spherical spectrum but are reorganised when a 3D structure is used. In the time domain, the influence of the 3D anelastic structure is also mainly on the amplitude (as expected) but 4 hours after the earthquake (R3 train), the effect on the phase starts to be observed. For the first oscillation of this train, the amplitude of the QR19 seismogram is lower than that of the PREM seismogram. Yet, the amplitude of the QR19 + SAW12D seismogram is higher than that of the SAW12D seismogram. This shows that the Fréchet derivatives of these seismograms for the anelastic structure are clearly dependant on the 3D elastic model. This is also obvious on the spectrum, for example on mode ${}_0S_{29}$, for which the effect of 3D anelastic structure is small when computed with a 1D elastic structure, whereas there is a huge difference between the elastic and anelastic spectra when a 3D elastic structure is used.

5. Conclusions

[22] We have presented a tool to compute long-period seismograms in a non-asymptotic framework. This method enables us to take jointly into account the rotation, ellipticity and 3D elastic and anelastic structures. We show that the presence of both lateral variations for elastic and anelastic parameters yields non-linear effects on the seismic signal. Thus, analysis of the seismic waveform in the framework of structure tomography should consider jointly the two structural parameters that are the seismic velocity and intrinsic quality factor. Otherwise, 3D anelastic models may be biased by their 3D elastic reference. These conclusions had already been drawn by *Resovsky and Ritzwoller* [1994], but their method was too computationnally intensive to be used in inversion schemes.

[23] We draw attention to the fact that the method we presented does not require huge computation facilities since all the programs used run on a single common workstation, in very reasonable computation time. Once the modes are computed for a given model, the computation of a great number of long seismograms is fast. Thus, these seismograms should be very useful in new inversion schemes to reinvestigate the amplitude of large-scale variation of seismic velocities, and to investigate uncharted parameters as the intrinsic quality factor in the whole mantle. They might also allow the use of very anomalous data which are usually rejected in selection processes, but obviously contain critical information.

[24] **Acknowledgments.** We are grateful to Joseph Resovsky and Rudi Widmer for their useful remarks during the review process. They have helped improve this paper. We thank the GEOSCOPE team for providing us with the data used in this study. This is IPGP contribution 1877.

References

Clévédé, E., and P. Lognonné, Fréchet derivatives of coupled seismograms with respect to an anelastic rotating Earth, *Geophys. J. Int.*, *124*, 456–482, 1996.

Dahlen, F. A., and J. Tromp, *Theoretical Global Seismology*, 1025 pp., Princeton Univ. Press, Princeton, N. J., 1998.

Dziewonski, A., and D. L. Anderson, Preliminary reference Earth model, *Phys. Earth Planet. Int.*, *25*, 297–356, 1981.

Gilbert, F., and A. Dziewonski, An application of normal mode theory to the retrieval of structural parameters and source mechanism for seismic spectra, *Philos. Trans. R. Soc. London, Ser. A*, *278*, 187–269, 1975.

Lay, T., and H. Kanamori, Geometric effects of global lateral heterogeneity on long-period surface wave propagation, *J. Geophys. Res.*, *90*, 605–621, 1985.

Li, X.-D., and B. Romanowicz, Global mantle shear velocity model developed using non linear asymptotic coupling theory, *J. Geophys. Res.*, *101*, 22,245–22,272, 1996.

Lognonné, P., Normal modes and seismograms in an anelastic rotating Earth, *J. Geophys. Res.*, *96*, 20,309–20,319, 1991.

Lognonné, P., and E. Clévédé, *Normal Modes of the Earth and Planets*, edited by W. H. K. Lee, H. Kanamori, and P. C. Jennings, pp. 125–147, Int. Assoc. of Seismol. and Phys. of the Earth's Inter., Boulder, Colo., 2002.

Lognonné, P., and B. Romanowicz, Modelling of coupled normal modes of the Earth: The spectral method, *Geophys. J. Int.*, *102*, 365–395, 1990.

Masters, G., J. Park, and F. Gilbert, Observations of coupled spheroidal and toroidal modes, *J. Geophys. Res.*, *88*, 10,285–10,298, 1983.

Park, J., and F. Gilbert, Coupled free oscillations of an aspherical, dissipative, rotating Earth: Galerkin theory, *J. Geophys. Res.*, *91*, 7241–7260, 1986.

Resovsky, J. S., and M. H. Ritzwoller, Characterizing long-period seismic effects of long-wavelength elastic and anelastic models, *Geophys. J. Int.*, *117*, 365–393, 1994.

Romanowicz, B., A global tomographic model of shear attenuation in the upper mantle, *J. Geophys. Res.*, *100*, 12,375–12,394, 1995.

Selby, N. D., and J. H. Woodhouse, The Q structure of the upper mantle: Constraints from Rayleigh wave amplitudes, *J. Geophys. Res.*, *107*, 2097, doi:10.1029/2001JB000257, 2002.

Woodhouse, J. H., and F. A. Dahlen, The effect of a general aspherical perturbation on the free oscillations of the Earth, *Geophys. J. R. Astron. Soc.*, *53*, 335–354, 1978.

Woodhouse, J. H., and Y. K. Wong, Amplitude, phase and path anomalies of mantle waves, *Geophys. J. R. Astron. Soc.*, *87*, 753–773, 1986.

Zürn, W., G. Laske, and F. Gilbert, Observation of Coriolis coupled modes below 1 mHz, *Geophys. J. Int.*, *143*, 113–118, 2000.

P. Lognonné and R. Millot-Langet, DGSP, IPGP, 4, avenue de Neptune, 94107 Saint-Maur, France. (lognonne@ipgp.jussieu.fr; rmillot@ipgp.jussieu.fr)

E. Clévédé, Département de Sismologie, IPGP, 4, place Jussieu - case 89, 75252 Paris Cedex 05, France. (clevede@ipgp.jussieu.fr)